Optical quality ZnSe films and low loss waveguides on Si substrates for mid-infrared applications

VINITA MITTAL, NEIL P SESSIONS, JAMES S WILKINSON AND GANAPATHY SENTHIL MURUGAN*

Optoelectronics Research Centre, University of Southampton, Southampton, SO17 1BJ United Kingdom
** smg@orc.soton.ac.uk*

Abstract: Zinc Selenide (ZnSe) is a promising mid-infrared waveguide material with high refractive index and wide transparency. Optical quality ZnSe thin films were deposited on silicon substrates by RF sputtering and thermal evaporation, and characterized and compared for material and optical properties. Evaporated films were found to be denser and smoother than sputtered films. Rib waveguides were fabricated from these films and evaporated films exhibited losses as low as 0.6 dB/cm at wavelengths between 2.5 µm and 3.7 µm. The films were also used as isolation/lower cladding layers on Si with $GeTe_4$ as the waveguide core and propagation losses were determined in this wavelength range.

OCIS codes: (310.1860) Deposition and fabrication, (230.7370) Waveguides, (140.3600) Lasers, tunable, (300.6340) Spectroscopy, infrared

References

1. K. Katayama, H. Matsubara, F. Nakanishi, T. Nakamura, H. Doi, A. Saegusa, T. Mitsui, T. Matsuoka, M. Irikura, T. Takebe, S. Nishine, T. Shirakawa, "ZnSe-based white LEDs,'' J. Cryst. Growth. **214/215**, 1064-1070 (2000).
2. H. Jeon, J. Ding, A. V. Nurmikko, W. Xie, D. C. Grillo, M. Kobayashi, R. L. Gunshor, G. C. Hua, and N. Otsuka, "Blue and green diode lasers in ZnSe-based quantum wells,'' Appl. Phys. Lett. **60,** 2045-2047 (1992).
3. D. W. Parent, A. Rodriguez, J. E. Ayers and F. C. Jain, "Photo-assisted MOVPE grown (n) ZnSe/(p+) GaAs heterojunction solar cells,'' Solid-State Electron. **47**(4), 595-599 (2003).
4. A. Lancaster, G. Cook, S. A. McDaniel, J. Evans, P. A. Berry, J. D. Shephard, and A. K. Kar, "Mid-infrared laser emission from Fe: ZnSe cladding waveguides'' Appl. Phys. Lett. **107**(3), 031108 (2015).
5. P. Gashin, A. Focsha, T. Potlog, A. V. Simashkevich, and V. Leondar, " n-ZnSe/p-ZnTe/n-CdSe tandem solar cells,'' Sol. Energy Mater. Sol. Cells. **46**(4), 323-331 (1997).
6. Y. Cheng, J. Lv, and F. Chen, "Mid-infrared ZnSe ridge waveguides fabricated by swift Kr^{8+} ion irradiation combined with precise diamond blade dicing,'' Opt. Mater. Express. **5**(10), 2292-2299 (2015).
7. J. R. Macdonald, R. R. Thomson, S. J. Beecher, N. D. Psaila, H. T. Bookey and A. K. Kar, "Ultrafast laser inscription of near-infrared waveguides in polycrystalline ZnSe,'' Opt. Lett. **35**(23), 4036-4038 (2010).
8. Y. Jia, and F. Chen, "Optical channel waveguides in ZnSe single crystal produced by proton implantation,'' Opt. Mater. Express. **2**(4), 455-460 (2012).
9. C. S. Riccardi, D. W. Hess and B. Mizaikoff, "Surface modified ZnSe waveguides for label-free infrared attenuated total reflection detection of DNA hybridization,'' Analyst. **136**(23), 4906-4911 (2011).
10. M. Kühnelt, T. Leichtner, S. Kaiser, B. Hahn, H. P. Wagner, D. Eisert, G. Bacher and A. Forchel, "Quasiphase matched second harmonic generation in ZnSe waveguide structures modulated by focused ion beam implantation,'' Appl. Phys. Lett. **73,** 584-586 (1998).
11. B.G. Kim, E. Garmire, N. Shibata and S. Zembutsu, "Optical bistability and nonlinear switching due to increasing absorption in single-crystal ZnSe waveguides,'' Appl. Phys. Lett. **51**(7), 475-477 (1987).
12. S. Venkatachalam, D. Mangalaraj and S. K. Narayandass, "Influence of substrate temperature on the structural, optical and electrical properties of zinc selenide (ZnSe) thin films,'' J. Phys. D: Appl. Phys. **39**(22), 4777 (2006).
13. A. Rizzo, M. A. Tagliente, L. Caneve and S. Scaglione, "The influence of the momentum transfer on the structural and optical properties of ZnSe thin films prepared by RF magnetron sputtering,'' Thin Solid Films. **368**(1), 8-14 (2000).
14. S. Venkatachalam, D. Mangalaraj, S. K. Narayandass, S. Velumani, P. Schabes-Retchkiman and J. A. Ascencio, "Structural studies on vacuum evaporated ZnSe/p-Si Schottky diodes,'' Mater. Chem. Phys. **103**(2), 305-311 (2007).

15. A. Rizzo, L. Caneve, S. Scaglione and M. A.Tagliente, “Structural and optical properties of zinc selenide thin films deposited by RF magnetron sputtering,’’ Proc. SPIE. **3738**, 40-47 (1999).
16. W. Gao, “Spectroscopic ellipsometry studies on vacuum evaporated zinc selenide thin film,’’ Proc. SPIE. **7283**, 72832L (2009).
17. V. H. Méndez-García, M. López-López and I. Hernández-Calderón, “ZnSe epitaxial films grown by MBE on nitrogen treated Si (111) substrates,’’ Superficies y vacío. **8**, 46-50 (1999).
18. J. Midwinter, “On the use of optical waveguide techniques for internal reflection spectroscopy,’’ IEEE J. Quant. Electron. **7**(7), 339-344 (1971).
19. J. T. Bradshaw, S. B. Mendes and S. S. Saavedra, “Planar integrated optical waveguide spectroscopy,’’ Anal. Chem. **77**(1), 28-A (2005).
20. M. Sieger and B. Mizaikoff, “Toward On-Chip Mid-Infrared Sensors,’’ Anal. Chem**. 88**(11), 5562-5573 (2016).
21. V. Mittal, A. Aghajani, L. G. Carpenter, J. C. Gates, J. Butement, P. G. Smith, J. S. Wilkinson. And G. S. Murugan, “Fabrication and characterization of high contrast mid-infrared $GeTe_4$ channel waveguides,’’ Opt. Lett. **40**(9), 2016-2019 (2015).
22. M. Ohring, *Film formation and structure. The material science of thin films*, (Academic, 1991).
23. V. Balan, C. Vigreux and A. Pradel, “Chalcogenide thin films deposited by radio-frequency sputtering,’’ J. Optoelectron. Adv. Mater. **6**, 875-882 (2004).
24. S. Antohe, L. Ion, M. Girtan and O. Toma, “Optical and morphological studies of thermally vacuum evaporated ZnSe thin films,’’ Rom. Rep. Phys. **65**(3), 805-811 (2013).
25. M. Özkan, N. Ekem, M. Z. Balbag and S. Pat, “ZnSe nanocrystalline thin films deposition on Si substrate by thermionic vacuum arc.,’’ in Proceedings of the Institution of Mechanical Engineers, Part L: J. Materials: Design and Applications, (Sage, 2012), pp.103-109.
26. M.W. Cho, K. W. Koh, K. Morikawa, K. Arai, H. D. Jung, Z. Zhu, T. Yao and Y. Okada, “Surface treatment of ZnSe substrate and homoepitaxy of ZnSe,’’ J. Electron. Mater. **26**(5), 423 (1997).
27. D. W. Hewak, D. Brady, R. J. Curry, G. Elliott, C. C. Huang, M. Hughes, K. Knight, A. Mairaj, M. N. Petrovich and R. E. Simpson, “Chalcogenide glasses for photonics device applications,’’ in *Photonic Glasses and Glass-Ceramics*, Murugan, G. S., ed. (Research Signpost, 2010).
28. D.T.F. Marple, “Refractive index of ZnSe, ZnTe, and CdTe,’’J. Appl. Phys. **35**(3), 539-542 (1964).
29. R. K. Watts, M. de Wit and W. C. Holton, “Nonoxide chalcogenide glass films for integrated optics,’’ Appl. Opt. **13**(10), 2329-2332 (1974).
30. J. Hu, V. Tarasov, A. Agarwal, and L. Kimerling, “Fabrication and testing of planar chalcogenide waveguide integrated microfluidic sensor,’’ Opt. Express **15**(5) 2307-2314 (2007).
31. C. Vigreux, R. Escalier, A. Pradel, L. Bastard, J.E. Broquin, X. Zhang, T. Billeton, G. Parent, M. Barillot and V. Kirschner, “Telluride buried channel waveguides operating from 6 to 20µm for photonic applications,’’ Opt. Mater. **49**, 218-223 (2015).
32. D. R. Scherer, J. M. Hensley, K. R. Parameswaran, B. D. Casse, V.Singh, P. T. Lin, A. Agarwal, L. C. Kimerling, J. Giam-marco, J. Wilkinson and I. Luzinov, “ Characterization of mid-infrared interband cascade laser coupling to a GeSbS chalcogenide glass waveguide,’’ Conference on Lasers and Electro-Optics, OSA Technical Digest (Optical Society of America,, 2012), paper CM4M.4.
33. A. Gutierrez-Arroyo, E. Baudet, L. Bodiou, J. Lemaitre, I. Hardy, F. Faijan, B. Bureau, V. Nazabal and J. Charrier, “Optical characterization at 7.7 µm of an integrated platform based on chalcogenide waveguides for sensing applications in the mid-infrared,’’ Opt. Express. **24**, 23109-23117 (2016).
34. G. M. Lohar, S. K. Shinde and V. J. Fulari, “Structural, morphological, optical and photoluminescent properties of spray-deposited ZnSe thin film,’’ J. Semicond. **35**(11), 113001 (2014).
35. V. Mittal, J. S. Wilkinson and G. S. Murugan, “High contrast $GeTe_4$ waveguides for mid-infrared biomedical sensing applications, ‘’ Proc. of SPIE, **8988,** 89881A-1 (2014).
36. D. Chandler-Horowitz and P. M. Amirtharaj, “High-accuracy, midinfrared ($450\ cm^{-1} \leq \omega \leq 4000\ cm^{-1}$) refractive index values of silicon,’’ J. Appl. Phys. **97**, 123526 (2005).

1. Introduction

Zinc selenide (ZnSe) is a chemically stable and non-hygroscopic group II-VI metal chalcogenide which possesses many useful semiconducting and optical properties, making it an important optoelectronic material. It has useful electronic properties such as a wide and direct bandgap, low electrical resistivity and n-type conductivity. The important optical properties such as broad transparency from visible to mid infrared (MIR) wavelengths, high refractive index, low dispersion and high photosensitivity combined with electronic properties have been exploited in many optoelectronic devices such as LEDs, laser diodes, MIR sources, solar cells [1-5] and optical windows, lenses and prisms. Low-loss waveguides have been realized in ZnSe substrates by methods such as diamond dicing [6], laser writing [7], proton implantation [8] and a macroscopic Fourier transform infrared-attenuated total reflection (FTIR-ATR) waveguide element has been used for the detection of DNA hybridization [9].

Epitaxial ZnSe thin films are usually grown on GaAs substrates to achieve lattice matching (0.27% mismatch) for applications in laser diodes [2], solar cells [3], second harmonic generation [10] and nonlinear switching [11]. However, the deposition of non-epitaxial several microns thick films of ZnSe on silicon (Si) is challenging mainly because of dissimilar thermal expansion and distinct chemical properties [12]. Studies of the microstructure of thin ZnSe films deposited on Si [13], of the influence of substrate heating on structural, optical and electronic properties of the ZnSe film deposited on Si [12,14-15], of UV to IR ellipsometry of ZnSe films deposited on Si [16] and of epitaxial film of ZnSe deposited on Si by MBE [17] have been reported. However, MBE is not suitable for growing thicker films of the order of a few microns. Therefore, in this paper, we report the deposition of ZnSe films of thicknesses between 1.9 and 4.5 µm on Si substrates by thermal evaporation and sputtering. The ZnSe film is used as a waveguide core on oxidized silicon and also as a lower cladding layer on Si, with $GeTe_4$ as the waveguide core for the MIR.

The fundamental absorption of biological molecules is orders of magnitude stronger in the MIR than their overtone bands in the near-infrared, rendering it a useful spectral region for highly sensitive absorption spectroscopy. The MIR corresponds to wavelengths between 2 µm and 20 µm and is broadly categorized into two spectroscopic windows, the mid wavelength infrared (MWIR) region covering wavelengths from 2-5 µm and the long wavelength infrared (LWIR) region from 8-12 µm. The 5-8 µm region is dominated by water absorption and hence it is of limited use for biochemical sensing. Optical waveguides are the most sensitive form of ATR element [18, 19] and low loss waveguides in these regions are of interest for MIR absorption spectroscopy of chemical species [20]. In our earlier work, $GeTe_4$ chalcogenide waveguides on bulk ZnSe substrates were demonstrated in both the MWIR and LWIR regions. Ductile dicing was used to prepare the end facets as conventional end facet polishing was unsuitable due to the soft and brittle nature of chalcogenide materials [21]. MIR waveguides fabricated on Si substrates would have the advantage that silicon is a plentiful, high quality low-cost material and can be readily cleaved along crystalline planes, avoiding end facet polishing. In this work, ZnSe films were deposited on Si by both sputtering and evaporation and compared for their structural, morphological and optical properties. The optical quality of evaporated and sputtered ZnSe was tested as a waveguide core and as a lower cladding/isolation layer on Si with a higher refractive index ($GeTe_4$, n~3.3) core. Propagation losses were measured by capturing the scattering of light propagating along the waveguide using an infrared camera from 2.5 µm to 3.7 µm in the MWIR. This paper is divided into three sections; 1) deposition and characterization of ZnSe thin films by RF sputtering and evaporation, and their comparison. 2) Fabrication and characterization of waveguides with ZnSe films as waveguide cores on oxidized silicon (n~1.45) and 3) Fabrication and characterization of waveguides with ZnSe films (n~2.4) as lower cladding on Si with $GeTe_4$ as a waveguide core. In sections 2 and 3, waveguide propagation losses are calculated and compared for the sputtered and evaporated ZnSe films.

2. Deposition and characterization of ZnSe films

Si (100) was used as the substrate for waveguide fabrication but the following substrates were also used to deposit ZnSe for the film characterization: Silicon (Si 100) (2 cm x 2 cm, 4 cm x 4 cm), silicon with a 2.5 µm thermally grown silica layer (oxidized Si) (4 inch diameter circular wafer cut in half), Germanium (Ge) (1 inch diameter circular wafer) and glass slides. Si, oxidized Si and glass slides were cleaned in Piranha (H_2O_2: H_2SO_4) solution, washed with de-ionized water and rinsed with acetone and isopropanol (IPA). Ge substrates were rinsed with IPA alone. All samples were dried with dry nitrogen gas and finally cleaned in a plasma asher, (Tepla 300) in an oxygen atmosphere (O_2 600ml/min) at 1000 W of microwave power for 15 min. This process heated the samples to ~160° C, removing residual moisture from the sample surface.

2.1 RF sputtering (AJA Orion)

Cleaned substrates were mounted on a platen facing down towards the target. A three inch diameter ZnSe target made by CVD was used. Substrates were heated in the sputtering chamber at 250°C in an argon atmosphere for two hours before starting the deposition. A sputtering pressure of 5 mTorr and an RF power of 50 W were used to deposit the films in an argon flow of 15 sccm, resulting in deposition at a rate between 0.05 and 0.06 nm/s, during which the samples were rotated and maintained at 250°C. After the deposition, the samples were annealed in an argon atmosphere within the chamber at 250°C for 2 hours, and the chamber was then allowed to cool down to room temperature before the samples were removed. The final ZnSe film thickness for sputtered ZnSe waveguides on oxidized silicon was 1.9 ± 0.1 µm, and for ZnSe as isolation layer for $GeTe_4$ waveguides was 4.5 ± 0.2 µm.

2.2 Thermal evaporation (BOC Edwards E306a)

ZnSe pieces made by CVD were placed in a tantalum boat and the substrates were mounted on the platen, facing down towards this evaporation source. The substrates were rotated and heated by a halogen lamp at 250°C for 2 hours inside the chamber in vacuum before starting the deposition. After reaching a base pressure of 7×10^{-6} mbar the deposition was started, at a rate of 0.5-0.7 nm/sec, with the substrates maintained at 250°C; the tantalum boat was held at an estimated temperature of 550°C. In order to keep the chamber pressure below $5\text{x}10^{-5}$, the deposition was performed in steps, depositing 1 µm thick film at a time and then leaving the samples inside the chamber at 250°C for approximately one hour to allow the pressure to fall again, before starting the next deposition step. This is equivalent to vacuum annealing of the samples to release thermal stresses built during the formation of the film. Once the required thickness was achieved, the samples were annealed in the chamber at 250°C for a further additional two hours and then allowed to cool to room temperature before the chamber was opened. The samples were heated or cooled slowly in steps of 30-50°C, to avoid peeling of the films. The final ZnSe film thickness for evaporated ZnSe waveguides on oxidized silicon was ~1.9 ± 0.2 µm, and that of ZnSe as isolation layer for $GeTe_4$ waveguides was ~ 4.1 ± 0.3 µm.

In preliminary attempts to deposit ZnSe, room temperature deposition was performed for both sputtered and evaporated films. However, in both cases, ~4 µm thick films flaked off during subsequent processing steps. Therefore, in this work, substrate heating was used during deposition to promote adhesion of the films to substrates. The evaporated films also needed further annealing to remove stresses for further processing of the films into waveguides. The evaporated samples were annealed in an annealing furnace at 280°C for two hours in an argon atmosphere. The sputtered films survived all the processing steps without peeling off which suggests that they had lower stresses than the evaporated films as they were deposited 10 times more slowly than the evaporated films. Furthermore, sputtered ZnSe film samples cracked after annealing under similar annealing conditions to evaporated samples (See Appendix 1.1) and so the annealing step was omitted for sputtered samples.

2.3 Material characterization

To realize low loss waveguides it is important to control the crystallinity, surface roughness, composition, transparency and refractive index of the materials. Crystal structure was determined by X-ray diffraction (XRD, Rigaku) with a monochromatic Cu kα target in 2 theta geometry. The morphology of the films was studied using field emission scanning electron microscopy (FESEM, Jeol) operating at voltages of 2-5 kV. The roughness of the deposited films was measured by atomic force microscopy (AFM, Veeco) in tapping mode. Compositional analysis was performed by X-Ray photoelectron spectroscopy (XPS, Thermoscientific). Optical transmission was determined by Fourier transform infrared spectroscopy (FTIR, Agilent 670) operating at wavelengths of 1.6-20 µm. The refractive index and propagation loss of the ZnSe films were determined using a prism coupler (MetriconTM) operating at 1550 nm. An optical parametric oscillator (OPO, M-Squared Lasers Firefly) and an infrared camera (FLIR A6540sc) were used to characterize the waveguides for guided modes and propagation loss in the mid-infrared wavelength region between 2.5 and 3.7 µm.

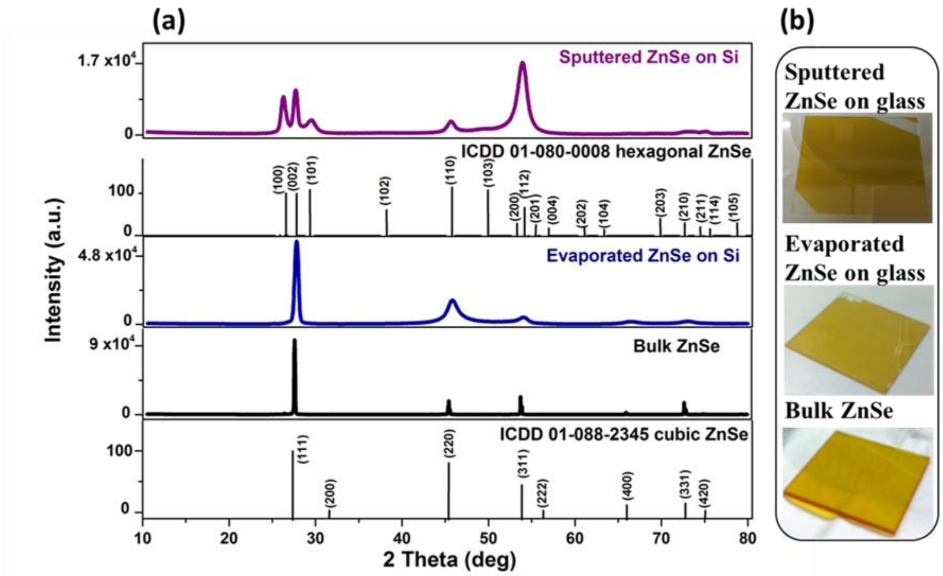

Fig. 1 (a) XRD patterns and (b) sample photographic images of ZnSe films deposited on glass substrates and bulk ZnSe substrate

2.3.1 Structural studies

The crystallinity of the deposited ZnSe films and commercially sourced bulk ZnSe substrate were determined by grazing incidence X-ray diffraction (GIXRD) with a grazing angle of 1° and 2θ in the range of 10°-80°. Fig 1 (a) shows the XRD patterns for sputtered, evaporated and bulk ZnSe along with the International Center for Diffraction Data (ICDD) crystal plane data for hexagonal and cubic ZnSe. All three measured ZnSe samples are polycrystalline but they differ in crystal structure. The sputtered ZnSe film shows mixed phases of wurtzite hexagonal and zinc blende cubic crystal structures as observed in [13] in which ZnSe was also deposited on Si by RF magnetron sputtering and the films were found to be in tensile, compressive or a mixture of both residual stresses depending on deposition pressure and power. On the other hand both the evaporated ZnSe film and bulk ZnSe show only cubic zinc blende crystal structure where the grains are mainly oriented towards [111] axis perpendicular to the coating surface. Thermal evaporation of ZnSe generally yields cubic polycrystalline films [12, 14] in line with the results obtained here. For waveguide applications, amorphous or small grain polycrystalline films are desirable. We obtained polycrystalline films for both sputtering and evaporation, with the evaporated films showing grain size significantly smaller than the sputtered films as shown by the SEM and AFM results (Fig. 2). Fig 1 (b) shows sample photographic images of ZnSe films deposited on glass substrates by sputtering and evaporation, and of a bulk ZnSe substrate. Visual examination shows that the deposited films resemble the bulk substrate in color indicating that the band edge of the deposited films lies in the visible region as expected and hence indicating the stoichiometry of the films. Both the sputtered and evaporated films were found to be hydrophilic with a contact angle of 30.5° and 88° respectively, when measured with de-ionized water (See Appendix 1.2).

2.3.2 Morphology and microstructure

FESEM was used to examine the microstructure of the films. Fig. 2 (a) shows a FESEM image of the surface, and (b) of the cross-section, of a sputtered ZnSe film on Si. The large grains of the sputtered films can be seen clearly and this may be due to the long duration of the films at 250°C in the deposition chamber. The film cross-section reveals the columnar void structure which can be explained by Thornton's zone model [22]; a similar structure for sputtered chalcogenide films is reported in [23]. These columnar structures could also be the reason for hydrophilic nature of the surface thereby attracting and trapping water vapors from atmosphere. Fig. 2 (c) and (d) shows FESEM images of the surface and cross-section of the evaporated ZnSe film on Si. The evaporated film shows more densely packed structures than the sputtered film, but contains some random circular spots which were also observed in [24-25]. These may be caused by "spitting", where a sudden release of impurities such as carbon or oxygen trapped in the source material leads to ejection of larger pieces of source material towards the samples. FESEM results confirm that the evaporated films are denser than the sputtered films. FESEM images also indicate that the sputtered films are rougher than the evaporated films, but in order to quantify the roughness of films, an AFM in tapping mode was used. The average roughness of the sputtered and evaporated films was determined over a 2 µm x 2 µm area as shown in Fig. 2 (e) and (f) respectively. The average roughness of the sputtered film is ~18.5 nm and that of evaporated film was found to be ~4 nm.

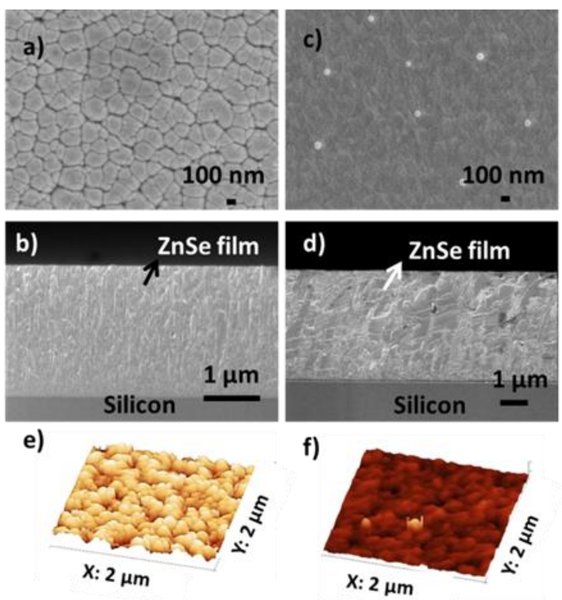

Fig. 2 FESEM images of surface and cross-section of sputtered (a), (b) and evaporated (c), (d) ZnSe film on Si. AFM image of a 2x2 μm^2 scan area of (e) sputtered and (f) evaporated ZnSe film on Si

2.3.3 Compositional analysis

XPS is a surface sensitive compositional measurement technique, and depth profiling enables acquisition of XPS spectra from a fresh surface exposed by in situ Ar ion beam etching of the film surface. XPS with a monochromatic Al Kα X-ray source (hv = 1486.6 eV) operating at a base pressure of 2×10^{-9} mbar was used to determine the composition of the ZnSe films. The X-ray source was operated at 6.7 mA emission current and 15 kV anode bias with a spot size of 400 µm and photoelectrons were collected over a cone of ±30° with the lens mounted at

40° with respect to the sample surface. For depth profiling, Ar ions with a current of 1 µA and 3 kV energy were used to etch the sample surface. XPS analysis was carried out on the unetched surface, and then after each of four 1 minute etching steps. Each minute of etching corresponds to ~ 4 nm etch depth.

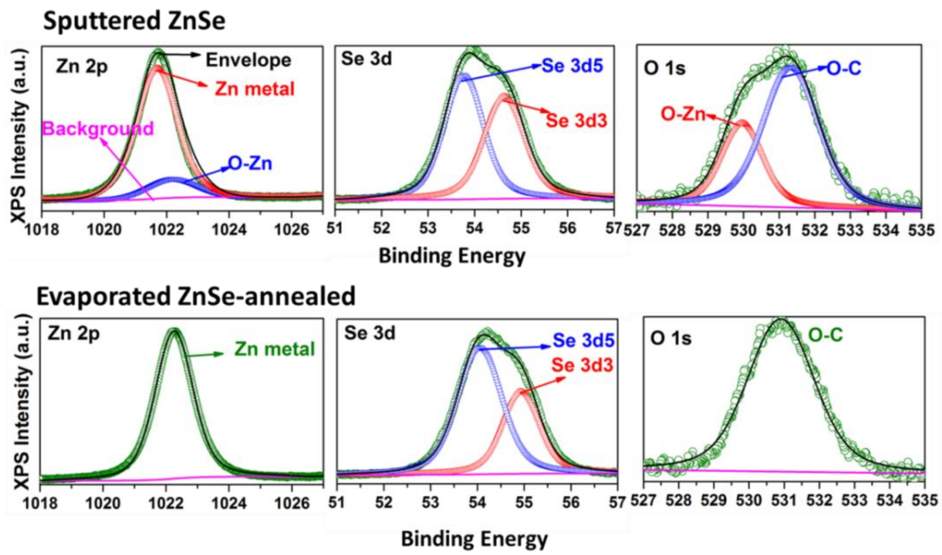

Fig. 3 XPS Spectra of sputtered and evaporated ZnSe films showing fitted peaks for the elements Zn, Se and O.

Carbon 1s core level at 284.8 eV was used as reference for correcting the charge shift. The data was analyzed using the Avantage software package (Thermo-Fisher Scientific). Fig. 3 shows the high resolution XPS surface spectra of core levels zinc (Zn 2p), selenium (Se 3d) and oxygen (O 1s) for both the as-deposited sputtered and the annealed evaporated films on Si. The experimental data points are shown as green circles, and the black curves show the best Gauss-Lorentz fit to the peaks. For quantitative compositional analysis, the background (magenta curve) was subtracted and the contributions from individual elements were fitted as indicated by the arrows in Fig. 3. The composition was determined by integrating the area under the individual peaks and normalizing these by the sensitivity factor for each element. The XPS scan of the sputtered film shows the presence of two Zn3p peaks, a high binding energy (B.E.) peak corresponding to zinc oxide (ZnO) and a low B.E. peak corresponding to metallic Zn [26]. In the O1s scan, two oxide peaks are shown, corresponding to a bonded ZnO peak and a non-bonded oxygen peak attached to organic carbon (O-C) or metal carbonates as shown in Fig 3. The evaporated ZnSe shows a single oxide peak corresponding to non-bonded oxygen along with Zn and Se. Presence of non-bonded oxygen is mainly due to surface contamination which could be avoided by capping the films with a protective coating soon after the deposition whereas the bonded oxygen present throughout the film affects the optical performance due to specific absorption of the metal oxide formed.

The results of depth profiling for both sputtered and evaporated films are reported in Table 1. The XPS analysis shows that the top layer of the sputtered ZnSe film is comprised of bonded and non-bonded oxygen as explained above. As the surface was etched further, a significant decrease in non-bonded oxygen was observed (from 18.38% to 2.45%) and after etching by ~4 nm, only the oxygen bonded to Zn was present. An oxide peak in the Zn 2p scan was also observed, but no evidence of the presence of SeO_2 was obtained, which has absorption peaks at 2.92 µm and 3.52 µm in the MIR region [27]. After etching by ~16 nm, ~

2.5% oxygen in the form of ZnO was still present in the sputtered film. On the other hand, non-bonded oxygen was present only in the top ~8 nm of the evaporated film and the film is free from any metal bonded oxides. The results clearly indicate the evaporated film is purer than the sputtered films in terms of oxygen contamination. The bonded oxygen which is present in the sputtered films is hard to remove as it is bonded to Zn. After observing oxide impurity in the films, the MIR absorption spectra of the films were measured before fabricating the waveguides.

Table 1. Composition analysis using XPS depth profiling of sputtered and evaporated ZnSe films

Element	Peak B.E (eV)	No etch Atomic %	1 min etch Atomic %	2 min etch Atomic %	3 min etch Atomic %	4 min etch Atomic %
Sputtered ZnSe						
Zn 2p	1022.1	30.67	36.08	44.73	45.82	46.63
Se 3d5	54.8	41.82	53.67	52.0	51.34	50.80
Se 3d3	53.95					
O 1s (ZnO)	529.8	9.12	7.81	3.27	2.85	2.57
Evaporated ZnSe						
Zn 2p	1022.26	40.47	42.82	44.85	45.14	44.94
Se 3d5	54.93	27.89	55.70	55.15	54.86	55.06
Se 3d3	54.04					
O 1s (O-C, metal carbonates)	531.3	18.38	2.45	-	-	-

2.3.4 Optical transmission

The optical transmission of the sputtered (2.9 µm thick) and evaporated (4.1 µm thick) ZnSe films deposited on Ge substrates and of the bulk ZnSe (2 mm thick) and Ge substrates (1 mm thick), polished on both sides, was measured using normal incidence FTIR. A resolution of 4 cm^{-1} averaged over 64 scans over the wavelength range 1.6 µm to 16 µm was used. Ge was chosen as the substrate for the film transmission measurements due to its wide transparency in the mid-infrared region. First, the transmission spectrum of a bare Ge substrate was taken and is shown as the red curve in Fig. 4. Then the transmission spectrum for the ZnSe film deposited on an identical Ge substrate was recorded, and the two spectra were ratioed to obtain the transmission spectrum of the ZnSe film alone, which is shown as the blue (evaporated) and purple (sputtered) curves in Fig. 4. The transmission spectrum of a bulk ZnSe substrate alone (black curve) is also shown in Fig. 4. The evaporated and sputtered film is transparent up to 15-16 µm in agreement with the bulk ZnSe.

2.3.5 Waveguiding, refractive index and loss

The refractive indices of the deposited films and the respective effective indices of the propagating modes and the propagation loss were determined using a Metricon^{TM} automatic prism-coupler (prism code 6024.3) at a wavelength of 1550 nm. Due to the high optical quality of oxidized silicon and the low absorption of silica at these wavelengths, ZnSe films

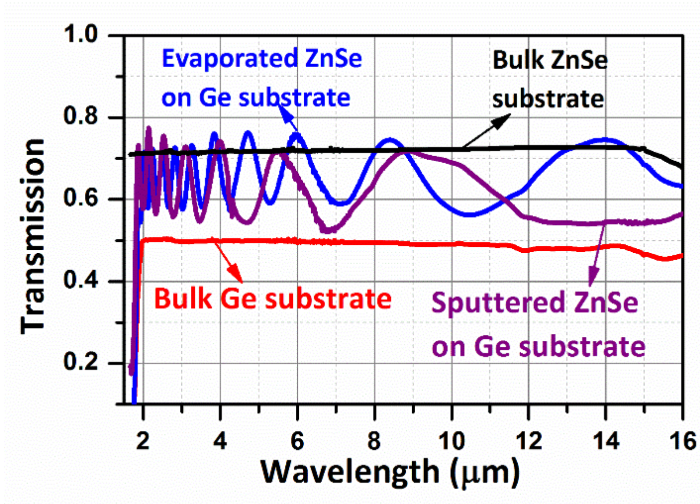

Fig. 4 Infrared transmission spectra of bulk ZnSe substrate, Ge substrate, sputtered and evaporated ZnSe films on Ge substrates.

deposited on oxidized silicon samples were used for these measurements, to assess film quality. The measured material refractive indices (n) of the ZnSe films in the TE polarization at 1550 nm wavelength are reported in Table 2 and are consistent with the values reported in the literature [28]. The propagation loss was measured by exciting the fundamental mode and scanning a fibre along the scattered streak of light in the direction of propagation, to determine the rate of decay of scattered power with respect to the distance along the waveguide. The effective refractive indices (N_{eff}), propagation losses of the fundamental modes and film thicknesses (t) are also given in Table 2, which shows that the evaporated ZnSe film has lower loss compared with the sputtered film, which is expected because the evaporated film is dense and has low surface roughness as shown by FESEM and AFM results. In the literature, the losses in chalcogenide slab waveguides on oxidized silicon substrates have been measured by prism coupling at $\lambda = 1.064$ μm to be 2, 10 and 20 dB/cm for As_2S_3, $Ge_{28}Sb_{12}Se_{60}$ and $Ge_{33}As_{12}Se_{55}$, respectively [29]. The propagation losses for fully etched channel waveguides of $Ge_{23}Sb_7S_{70}$ on oxidized Si was measured to be 2.3 dB/cm at $\lambda = 1.55$ μm [30].

Table 2. Prism coupling measurements for ZnSe films in TE polarization at 1550 nm

	n	N_{eff}	t (nm)	Loss (dB/cm)
Sputtered	2.4240 ±0.0001	2.395	1897.0	1.44
Evaporated	2.4239 ±0.0001	2.418	1893.0	1.16

3. ZnSe films as a waveguide core

Sputtered and evaporated samples with 1.9 µm thick ZnSe films on oxidized silicon were converted into rib waveguides by photolithography and Ar ion beam etching. S1813 photoresist (Shipley) was used to pattern the samples with straight ribs with widths from 1 to 20 microns. The samples were exposed using an i-line Hg lamp source with an exposure dose of 144 mWs/cm^2 and then developed in MIF 319 developer for 45 sec. The etch rate of ZnSe was ~ 50 nm/min with a beam current of 100 mA. Waveguide characterization was carried out for a waveguide with an etch depth (rib height) of 1.6 µm and the remaining slab thickness of 0.3 µm and a rib width ~20 µm, as shown in the SEM image of the sample cross-section in Fig. 5 (a). Light from the tunable OPO was coupled into the waveguide using a ZrF_4 fiber butt-coupled to the waveguide and the guided light was recorded using the mid-infrared camera. Fig. 5 (b) and (c) show top view images of the waveguide with guided light at a wavelength of 3.7 µm emerging from the waveguide end, for the sputtered and evaporated ZnSe films, respectively. Note that the color of the images is false and represents the hot and cold regions in the frame.

With light coupled into a waveguide, propagation loss was measured by recording an infrared image of the surface in a region 1-2 mm away from the input facet to capture the scattered light along the waveguide. This image was background corrected by subtracting an (otherwise identical) image with the laser turned off. This procedure was repeated for wavelengths between 2.5 µm and 3.7 µm at intervals of 0.1 µm. Fig 5 (d) shows the propagation loss calculated by fitting an exponential to the streak of light captured, as a function of wavelength. The error bars represents the standard deviation between three data points at each wavelength collected from three different but nominally identical waveguides. The minimum loss calculated in evaporated ZnSe waveguides is ~ 0.6 dB/cm at λ = 2.5 µm and 3.5-3.6 µm. The losses in sputtered ZnSe waveguides are between 5.3–11.75 dB/cm. The higher losses for the sputtered films are believed to be due to inadequate film quality, higher surface roughness and large grain size as well as columnar structures that may trap oxygen from the atmosphere and cause oxide impurities, as seen in the XPS analysis discussed above.

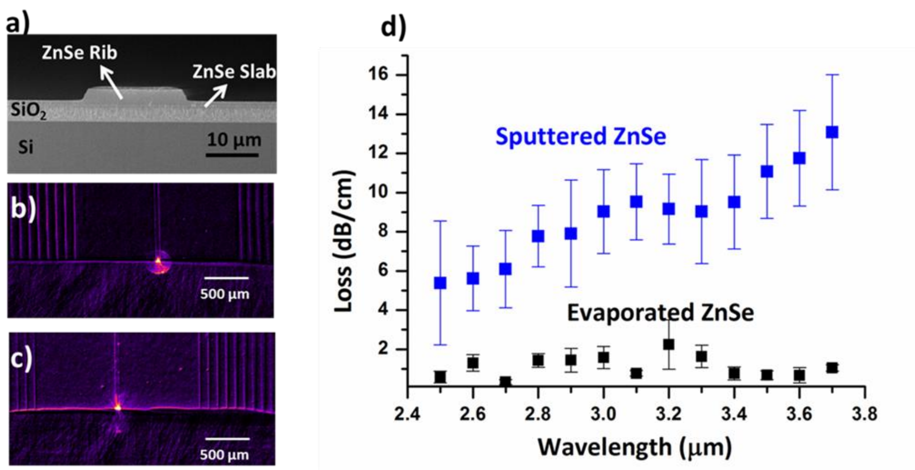

Fig. 5 (a) FESEM image of a cross-section of a ZnSe rib waveguide on oxidized Si, (b) and (c) IR images of the guided light emerging from the waveguide end, for the sputtered and evaporated ZnSe waveguides, respectively at λ = 3.7 µm, (d) propagation losses for the sputtered and evaporated ZnSe waveguides respectively, for λ = 2.5-3.7 µm.

For waveguides with thermal evaporated ZnSe, we expect to have lower losses at longer wavelengths because of the reduction in the Rayleigh scattering losses due to roughness. However, current ZnSe waveguides on oxidized Si are not suitable at wavelengths longer than

4 µm and efforts are underway to fabricate such waveguides on fluoride based materials, both on bulk substrates as well as thin film on Si substrates that will be able to guide light up to 10 µm of spectral region.

4. ZnSe films as waveguide isolation layers

Having established the fabrication of high quality low-loss ZnSe films, they were employed as isolation layers between the silicon substrate and a high index $GeTe_4$ core, with a view to achieving broadband MIR operation beyond the silica absorption edge at $\lambda \approx 4$ µm. Identical 20 µm wide fully etched, straight $GeTe_4$ channel waveguides of thickness 2.1 $\pm$0.2 µm were fabricated on both 4.5 µm thick sputtered and 4.1 µm thick evaporated ZnSe films on silicon. The thickness of isolation layer required to yield a loss into the silicon of <0.1 dB/cm was calculated by numerical modeling (see Appendix 1.3). The lift-off method was used to fabricate the $GeTe_4$ waveguides, as follows. A ~6 µm thick film of AZ2070 negative photoresist (Microchemicals) was spun onto the ZnSe/Si samples. After soft baking, the samples were exposed through a mask with straight lines having widths from 1 to 20 microns using an i-line Hg lamp source with an exposure dose of 56 mWs/cm^2 and then post exposure baked (PEB) to crosslink the exposed resist. They were then developed in AZ726 MIF developer for 2 min to create an undercut profile. $GeTe_4$ was then deposited on these patterned samples by RF sputtering at 40W sputtering power and 15 mTorr sputtering pressure [21]. The photoresist was then lifted off by soaking the samples in acetone, leaving the 20 µm wide $GeTe_4$ channels on the ZnSe film surface. Fig. 6 shows an SEM image of the cross-section of a $GeTe_4$ channel on a sputtered ZnSe film on Si after removing the photoresist. The trapezium like shape of the channels is due to non-directionality of the sputtering process. The waveguides were then characterized for propagation loss using scattered light images as described above in Section 2. The propagation loss was found to be 31±1 dB/cm and 25±3 dB/cm at $\lambda = 3.5$ and $\lambda = 3.7$ µm respectively for the sputtered ZnSe isolation layer and 13±1 dB/cm and 10±2 dB/cm for the evaporated ZnSe isolation layer. The higher losses in these waveguides are believed to be caused by oxide contamination of the $GeTe_4$ target used for sputtering the $GeTe_4$ films. However, these results confirm the lower loss of evaporated ZnSe films compared to sputtered ZnSe films when used as an isolation layer, in agreement with the results on ZnSe films and waveguides described in earlier sections. Work is underway to minimize these losses by using further purified raw materials to realize oxide free $GeTe_4$ films on ZnSe isolation layers on silicon.

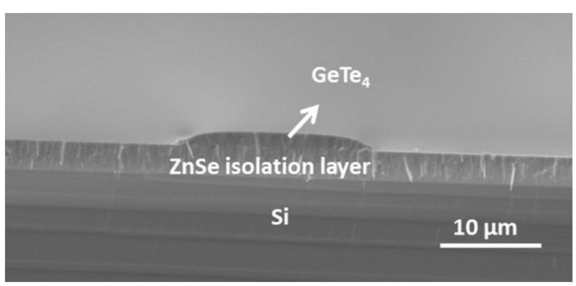

Fig. 6 FESEM image of cross-section of $GeTe_4$ channel waveguide on Si with a ZnSe isolation layer

Researchers working on a similar waveguide core materials recently reported a total insertion loss of -10.5 dB with a propagation loss of 6.6 dB/cm at $\lambda = 10$ µm for a $Ge_{17}Te_{83}$ buried channel waveguide (19 µm wide and 15 µm high) on a $Te_{75}Ge_{15}Ga_{10}$ substrate with a $Ge_{24}Te_{76}$ superstrate [31]. A chalcogenide ridge waveguide of $Ge_{23}Sb_7S_{70}$ core deposited by thermal evaporation on silica coated silicon showed a total insertion loss of -28 dB measured at $\lambda = 3.4$ µm [32]. Recently, a fully etched waveguide with a chalcogenide composition of GeSbSe showed propagation losses of 2.5 dB/cm at $\lambda = 7.7$ µm [33].

5. Conclusions

Optical quality ZnSe films of thickness up to 4.5 µm were deposited using both RF magnetron sputtering and thermal evaporation. These films were characterized for their structural and optical properties. Both of them were found to be polycrystalline with thermally evaporated ZnSe films being denser and smoother than sputtered films. Refractive indices of the sputtered and evaporated films were measured to be 2.4240 and 2.4239 at 1550 nm, respectively and are in good agreement with the CVD produced bulk starting material used. They were found to be transparent up to about 16 µm wavelength. Composition analysis proved that the sputtered films suffer from oxide contamination throughout the bulk of the film whereas the evaporated films have oxide contamination only at the surface which could be avoided using protective coatings. ZnSe films deposited on oxidized silicon wafers were fabricated in to rib waveguides by photolithography and Ar-ion beam etching. Waveguides made of thermally evaporated ZnSe films showed losses as low as 0.6 dB/cm at mid-IR wavelengths. Evaporated ZnSe was also demonstrated as a promising material as a low-loss isolation layer for mid-infrared waveguide applications.

Funding

This research is funded by the European Union’s Seventh Framework Programme (FP7/2007-2013) ERC grant agreement no. 291216 “Wideband Integrated Photonics for Accessible Biomedical Diagnostics”. (http://wipfab.southampton.ac.uk/)

Appendix

1.1 The FESEM and GIXRD results for a sputtered ZnSe film after annealing in Ar atmosphere for 2 hours at 280°C are shown in Fig. 7. The cracks in the films are clearly seen in Fig. 7 (a). On magnifying the ZnSe film surface further as shown in Fig 7 (b) and (c) the phase separation is clearly observed. The film has many large voids surrounded by large grains. GIXRD performed on the annealed film further confirmed that the grains are oriented in random planes as shown in Fig 7 (d).

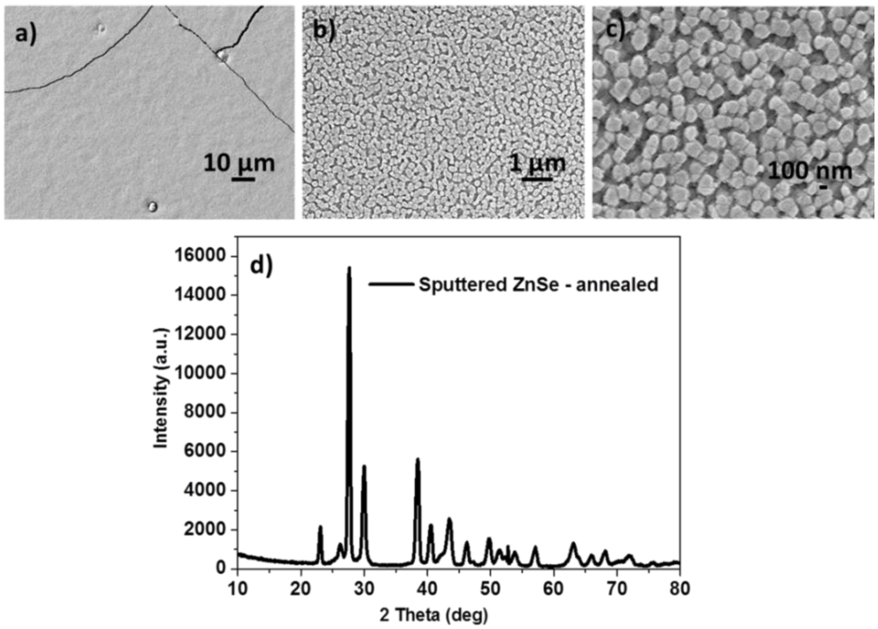

Fig. 7 (a), (b) and (c) FESEM image of surface and (d) XRD pattern of Sputtered ZnSe film deposited on Si after annealing

1.2 Surface wettability was measured by static contact angle measurement with deionized (DI) water on the deposited ZnSe films and on bulk ZnSe, with the angle between the water drop and the film surface being measured to define the hydrophilic or hydrophobic nature of the surface. This is governed by surface chemistry and roughness of the solid film. A hydrophilic surface has strong affinity to water therefore wets a large area of surface by maximizing the contact and has a contact angle less than 90°. A hydrophobic surface repels water and has a contact angle greater than 90°. Fig. 8 shows a water drop on each of the three ZnSe surfaces. The sputtered ZnSe was found to be hydrophilic with a contact angle of 30.5° whereas bulk ZnSe is hydrophobic in nature with a contact angle of 112°. The evaporated ZnSe was found to be closer to hydrophobic in nature with a contact angle of 88°. A contact angle of 65° was reported earlier for a 280 nm thick spray pyrolysis deposited ZnSe film [34].

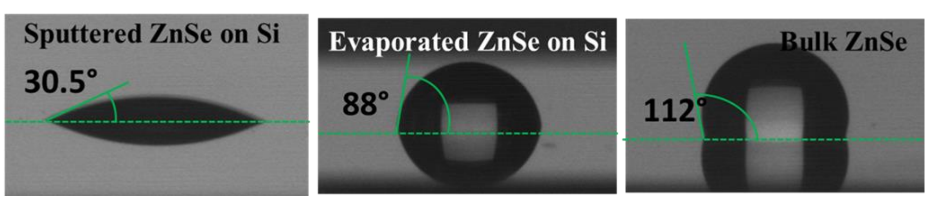

Fig. 8 Water contact angle of sputtered, evaporated and bulk ZnSe

1.3 A numerical waveguide model was used to determine the ZnSe isolation layer thickness, a_i, that would be required to reduce the tunneling loss into the silicon substrate to below 0.1 dB/cm for a $GeTe_4$ core waveguide, for wavelengths up to 10 µm. The waveguide core was approximated as a slab waveguide. The refractive index dispersion of $GeTe_4$ and ZnSe determined by ellipsometry [35], and the dispersion and absorption of Si from literature [36] were used in the model. The waveguide core thickness, a_c, was taken to be 2 µm, to achieve guidance throughout the MIR spectral window. Fig. 9 (a) shows a schematic of the waveguide showing the thickness and refractive indices of different layers. Fig. 9 (b) shows the fundamental mode field for a 2 µm thick $GeTe_4$ waveguide on Si at a wavelength of 3.5 µm. Fig. 9 (c) shows the dispersion of $GeTe_4$ and ZnSe and the effective indices of $GeTe_4$ waveguide on ZnSe, for the TE and TM polarizations. Fig. 9 (d) shows the thickness of ZnSe isolation layer needed between the $GeTe_4$ core and the Si substrate to achieve a propagation loss of 0.1 dB/cm for each polarization. It can be seen that the thickness of the isolation layer needed is higher for the TM polarization and increases at longer wavelengths, as expected. Based on these results we have chosen the thickness of the ZnSe isolation layer to be around 4.5 µm to enable characterization of $GeTe_4$ waveguides up to about 9 µm wavelength.

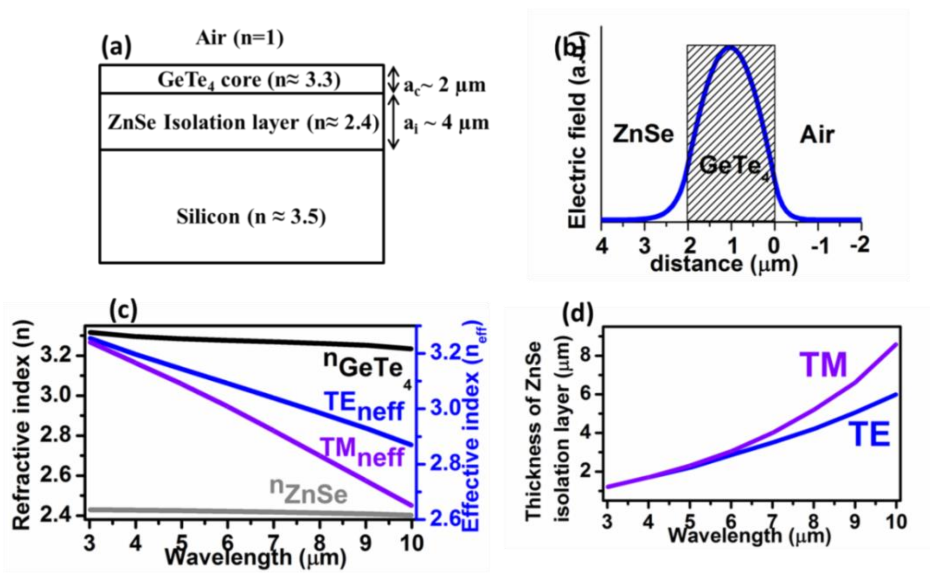

Fig. 9 (a) Schematic diagram of $GeTe_4$/ZnSe/Si slab waveguide design; (b) Mode field profile for a_c = 2 µm and a_i = 4 µm at λ = 3.5 µm; (c) waveguide material and effective indices vs wavelength, and (d) thickness τ for a propagation loss of 0.1 dB/cm, for both polarizations.